High resolution laser excitation spectroscopy of the $\tilde{B}\,^2E$-$\tilde{X}\,^2A_1$ transitions of calcium and strontium monoborohydride

M. J. Dick
Department of Physics, University of Waterloo, Waterloo, Ontario N2L 3G1, Canada

P. M. Sheridan[a] and J.-G. Wang[b]
Department of Chemistry, University of Waterloo, Waterloo, Ontario N2L 3G1, Canada

P. F. Bernath[b),c)]
Department of Physics, University of Waterloo, Waterloo, Ontario N2L 3G1, Canada and Department of Chemistry, University of Waterloo, Waterloo, Ontario N2L 3G1, Canada

(Received 22 January 2007; accepted 14 March 2007; published online 27 April 2007)

High resolution spectra of the $\tilde{B}\,^2E$-$\tilde{X}\,^2A_1$ transitions of $CaBH_4$ and $SrBH_4$ have been recorded using laser excitation spectroscopy in a laser ablation/molecular jet source. Because of rotational cooling in the molecular jet and nuclear spin statistics, transitions arising from only the $K'=1\leftarrow K''=0$, $K'=2\leftarrow K''=1$, and $K'=0\leftarrow K''=1$ subbands have been observed. For each molecule, an analysis of the data using ^2E and $^2A_1$ symmetric top Hamiltonians yielded rotational, spin-orbit, and spin-rotation parameters for the observed states. For both molecules the rotational constants compare well with those calculated for a tridentate borohydride structure. A large reduction in the spin-orbit splitting and in the metal-ligand separation for each molecule indicates an increase in the amount of d atomic orbital character in the first excited ^2E states of the monoborohydrides as compared to the monomethyl derivatives. For each molecule no evidence of internal rotation of the BH_4^- ligand was found. A change in the magnitude and sign of the spin-rotation constant ε_1 confirms an energy reordering of the first excited ^2E and $^2A_1$ states in both $CaBH_4$ and $SrBH_4$ as compared to $CaCH_3$ and $SrCH_3$. The data also suggest that the $\tilde{B}\,^2E_{1/2}$ rotational energy levels of $CaBH_4$ may be perturbed by a vibronic component of the $\tilde{A}\,^2A_1$ state. © *2007 American Institute of Physics*. [DOI: 10.1063/1.2723097]

I. INTRODUCTION

$CaBH_4$ and $SrBH_4$ are the only members of the isoelectronic $2p$ ligand family of molecules (CaF/SrF, CaOH/SrOH, $CaNH_2/SrNH_2$, and $CaCH_3/SrCH_3$)[1–6] that have not yet been observed using high resolution spectroscopy. From the previous investigations of the molecules in this series, the metal-ligand bonding has been found to be largely ionic and to occur between the metal cation and the heaviest atom of the negatively charged ligand. In contrast, the borohydride anion (BH_4^-), which possesses a tetrahedral structure, cannot form a bond directly between the central boron and metal atoms.[7,8] In this case, the metal-ligand bonding in the alkaline-earth borohydrides must occur through bridging hydrogens. As a result, three structures are possible, monodentate (one bridging hydrogen, C_{3v} symmetry), bidentate (two bridging hydrogens, C_{2v} symmetry), and tridentate (three bridging hydrogens, C_{3v} symmetry) (structures can be found in Ref. 9). In addition, the electronic structure of the molecules in the $2p$ ligand series has been well described in terms of a perturbation of the metal atomic orbitals by the ligand. The unique geometric configurations possible for the alkaline-earth borohydrides may disrupt this perturbation description and may have an affect on the excited state electronic structure, which makes them of particular interest for spectroscopic investigation.

One group of metal borohydrides that have been the subject of several studies, both theoretical and experimental, is the alkali metal borohydrides. The experimental work[9–18] has consisted primarily of microwave spectroscopic investigations in the gas phase. In these studies, the rotational and hyperfine parameters have been determined for the ground electronic states of $NaBH_4$,[9–12] $NaBD_4$,[10,13] $LiBH_4$,[10,14,15] $LiBD_4$,[13] and KBH_4.[11,13] Based on isotopic data, lithium and sodium borohydrides were found to possess the tridentate structure in the ground state. Theoretical studies[19–28] have also predicted this geometric configuration for the ground state. Additionally, several of these theoretical studies have calculated a low-energy barrier to the internal rotation of the ligand,[19,22–25,27,28] in which the BH_4^- cycles from one tridentate minimum to another through a bidentate intermediate structure. This phenomenon will manifest itself in the observed rotational spectra as a doubling of spectral lines.[29] In the rotational spectroscopic studies of the alkali metal boro-

[a)]Present address: Department of Chemistry and Biochemistry, Canisius College, Buffalo, New York, 14208-1098.
[b)]Present address: Department of Chemistry, University of York, Heslington, York, YO10 5DD, UK.
[c)]Author to whom correspondence should be addressed. Tel: +44-1904-434526; Fax: +44-1904-432516; Electronic mail: pfb500@york.ac.uk

hydrides, this doubling of spectral lines was not resolved, indicating that the barrier to the internal motion of the BH_4^- group is larger than that calculated.

Studies involving the alkaline-earth borohydrides have been far less extensive. Pianalto *et al.*[30] have used laser excitation and dispersed fluorescence experiments in a Broida oven to examine the $\tilde{A}\,^2A_1$-$\tilde{X}\,^2A_1$ and $\tilde{B}\,^2E$-$\tilde{X}\,^2A_1$ electronic transitions of $CaBH_4$ and $SrBH_4$ at low resolution. From their spectra, they suggested that these molecules possessed C_{3v} symmetry and a tridentate structure similar to the structure found later for the alkali borohydrides. Most interestingly, they found that the first excited $^2A_1$ and ^2E states appeared to be reversed in energy relative to the corresponding states in the metal monomethyls, $SrCH_3$[5,6] and $CaCH_3$.[6,31,32] Subsequently, Ortiz[33] used electron propagator methods to calculate the energy, vibrational frequencies, geometric structure, and orbital character of several electronic states of $CaBH_4$. From this work a tridentate structure was predicted for $CaBH_4$. However, the first excited ^2E and $^2A_1$ electronic states were found to be ordered in energy the same as in $CaCH_3$, contrary to the experimental work. In addition, Chan and Hamilton[34] have used density functional theory to calculate ground state geometries and vibrational frequencies for the monoborohydrides of calcium and strontium. In their work they also found that the tridentate structure was the lowest in energy in the ground electronic state.

In an attempt to further understand the geometric and excited state electronic properties of $CaBH_4$ and $SrBH_4$ and to reconcile the discrepancy between theory and experiment for $CaBH_4$, we have recorded high resolution laser excitation spectra of the $\tilde{B}\,^2E$-$\tilde{X}\,^2A_1$ transitions of both calcium and strontium monoborohydride. For each molecule the rotational and fine structure parameters have been determined for the ground and excited electronic states. These constants have conclusively established that the first two excited electronic states have reversed their order in energy relative to their MCH_3 analogs. A discussion of the geometry, energy ordering, and orbital character of the observed states will be presented. In addition, a comparison of the observed spectroscopic parameters with those of $SrCH_3$ and $CaCH_3$ will be described.

II. EXPERIMENT

A laser ablation/molecular jet source was used to produce the borohydrides of calcium and strontium in the gas phase.[35] First, a gas mixture was introduced into a reaction nozzle via a pulsed valve. For this synthesis a mixture of 5% diborane in argon (Praxair), at a backing pressure of 100 psi, was used as the reactant gas. Next, the third harmonic (355 nm) of a pulsed (10 Hz) neodymium-doped yttrium aluminum garnet laser (10 mJ/pulse) was used to vaporize a metal target rod (calcium or strontium) located in the nozzle. Inside the reaction region a high-energy plasma was formed. Here the diborane reacted with the metal vapor, producing the metal borohydrides. The molecules then exited into the low pressure chamber ($\sim 1\times 10^{-7}$ Torr), forming a molecular jet with a low rotational temperature ($T_{\mathrm{rot}}\sim 4-6$ K). A probe laser was then sent perpendicularly through the expansion ~15 cm downstream. The resulting molecular fluorescence was collected by a photomultiplier tube, sent through a preamplifier (100× current), and processed by a boxcar integrator. Bandpass filters (±20 nm) were used to help attenuate stray radiation from the ablation laser and plasma emission.

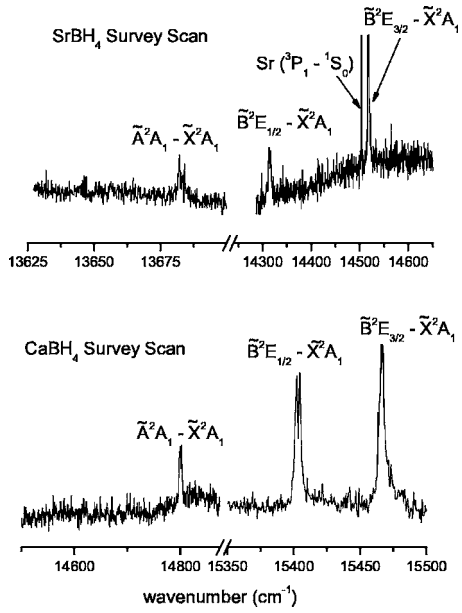

FIG. 1. Low resolution spectra recorded for the $\tilde{A}\,^2A_1$-$\tilde{X}\,^2A_1$ and $\tilde{B}\,^2E$-$\tilde{X}\,^2A_1$ transitions of $SrBH_4$ (upper panel) and $CaBH_4$ (lower panel). For each molecule the $\tilde{A}\,^2A_1$-$\tilde{X}\,^2A_1$ transition was weaker in intensity and located at a lower energy than the corresponding $\tilde{B}\,^2E$-$\tilde{X}\,^2A_1$ transitions. This energy ordering is in contrast to that of $CaCH_3$ and $SrCH_3$, but is consistent with the previous low resolution observation of calcium and strontium borohydrides.

Initially, low resolution survey scans were obtained using an argon-ion-pumped linear dye laser (linewidth ~30 GHz) scanned at a speed of ~50 cm^{-1}/min. DCM and pyridine 2 laser dyes were used to observe the spectral region of interest (~13 500–15 500 cm^{-1}) with a typical maximum output power of ~1 W (pump power ~5 W). A LABVIEW data acquisition program was used to plot the output signals from the boxcar integrator versus the wave number of the laser, which was obtained using a wavemeter (Burleigh WA-2500 Wavemeter Jr.) interfaced with the program.

For the $\tilde{B}\,^2E$-$\tilde{X}\,^2A_1$ transitions of both $CaBH_4$ and $SrBH_4$, an argon-ion-pumped Coherent Autoscan 699-29 ring dye laser system, operating with DCM laser dye, was used to obtain high resolution spectra [linewidth ~10 MHz, output power ~1 W (pump power ~8 W)]. Generally, spectra were obtained in 5 cm^{-1} portions at a scan rate of 180 s/cm^{-1} and a data sampling interval of 10 MHz. To achieve an adequate signal to noise ratio, several (2–4) portions were usually averaged together. The final spectra were then calibrated using the line positions of I_2 obtained from simultaneously recording its laser excitation spectra.[36]

III. RESULTS

Figure 1 shows low resolution survey spectra of the $\tilde{A}\,^2A_1$-$\tilde{X}\,^2A_1$ and $\tilde{B}\,^2E$-$\tilde{X}\,^2A_1$ transitions of $CaBH_4$ and $SrBH_4$. In each spectrum, three peaks are clearly present. For

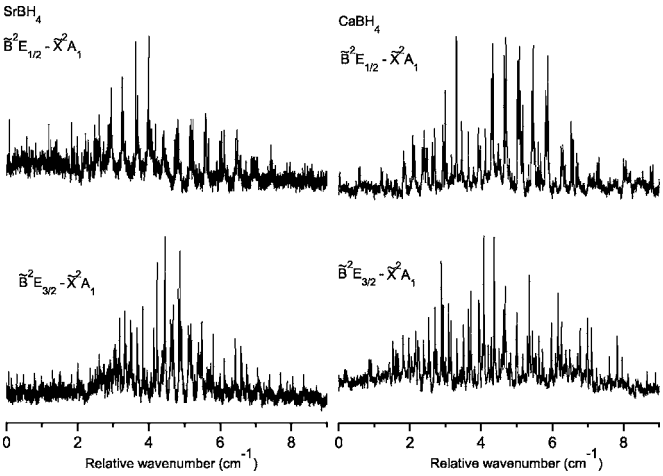

FIG. 2. High resolution spectra of the two spin-orbit components of the $\tilde{B}\,^2E$-$\tilde{X}\,^2A_1$ transition of $SrBH_4$ and $CaBH_4$ are plotted on a relative wavenumber axis scale for comparison. The $\tilde{B}\,^2E_{3/2}$-$\tilde{X}\,^2A_1$ spin-orbit component of $SrBH_4$ is shown in the bottom left panel. This component has an expected appearance similar to a Hund's case (a) $^2\Pi$–Hund's case (b) $^2\Sigma^+$ transition with $\sim 1B$ and $\sim 3B$ spaced branches. The $\tilde{B}\,^2E_{1/2}$-$\tilde{X}\,^2A_1$ spin-orbit component of $SrBH_4$ is shown in the top left panel. This component has a very unique structure with no clear origin, and all of the lines of the observed branches appear to be spaced by $\sim 2B$. Neither component of the $\tilde{B}\,^2E$-$\tilde{X}\,^2A_1$ transition of $CaBH_4$ (right side) has the appearance of a perpendicular transition. Each component is highly congested and lacks any clear origin, which hampered the rotational assignment of the lines in these spectra.

$CaBH_4$ the separation between the first and second peaks is $\sim 600\ cm^{-1}$, while the second and third peaks are spaced by $\sim 70\ cm^{-1}$. The $70\ cm^{-1}$ separation is in the range of the spin-orbit splitting previously measured for the $\tilde{A}$ states of CaF, CaOH, and $CaCH_3$.[1,2,6,31,32] This suggests that the second and third peaks are two spin-orbit components of an orbitally degenerate electronic state. This scenario is only possible if the molecule possesses a geometric configuration with C_{3v} symmetry. For a molecule having C_{2v} symmetry, such as $CaNH_2$,[37] no two of the first three excited states should be spaced by this $\sim 70\ cm^{-1}$ separation exhibited by calcium-containing molecules (C_{2v} symmetry eliminates first order spin-orbit coupling). Therefore, the wave number separations exhibited by the first three peaks for $CaBH_4$ suggest that C_{2v} symmetry is unlikely. A similar conclusion can be arrived at for $SrBH_4$, where the second and third peaks are spaced by $\sim 200\ cm^{-1}$. This separation is consistent with the previously observed spin-orbit splitting in the $\tilde{A}$ states of SrF, SrOH, and $SrCH_3$.[1–3,5] As a result, for the borohydrides the first excited $^2A_1$ state was found to lie lower in energy than the first excited ^2E state, consistent with the previous observations of the metal borohydrides.[30] It is also of interest to note the decreased intensity of the $\tilde{A}\,^2A_1$-$\tilde{X}\,^2A_1$ transitions as compared to the $\tilde{B}\,^2E$-$\tilde{X}\,^2A_1$ transitions in the spectra in Fig. 1. For each molecule the decreased signal strength was observed previously[30] and does not seem to be simply an effect of the lower laser power. The decrease in intensity of the $\tilde{A}\,^2A_1$-$\tilde{X}\,^2A_1$ transitions impeded the measurement of their high resolution spectra.

Figure 2 shows the overall high resolution spectra obtained for both spin-orbit components of the $\tilde{B}\,^2E$-$\tilde{X}\,^2A_1$ transitions of $CaBH_4$ and $SrBH_4$. The $\tilde{B}\,^2E$-$\tilde{X}\,^2A_1$ transitions correspond to a $p\pi \leftarrow s\sigma$ promotion on the calcium or strontium ion. Transitions of this type should have the general appearance of a Hund's case (a) $^2\Pi$–Hund's case (b) $^2\Sigma^+$ perpendicular transition of a corresponding linear molecule such as CaCCH[38,39] and SrCCH.[40] In this case two spin-orbit components, each with a well defined origin and $\sim 1B$ and $\sim 3B$ spaced branches, are present. For $SrBH_4$, the $\tilde{B}\,^2E_{3/2}$-$\tilde{X}\,^2A_1$ component (lower left panel) indeed exhibits the appearance of a perpendicular transition with $\sim 1B$ and $\sim 3B$ spaced branches. The $\tilde{B}\,^2E_{1/2}$-$\tilde{X}\,^2A_1$ component (upper left panel), on the other hand, exhibits a pattern that closely resembles a parallel transition with only $\sim 2B$ spaced branches present. For the $\tilde{B}\,^2E$-$\tilde{X}\,^2A_1$ transition of $CaBH_4$, neither spin-orbit component (top or bottom right panel) has the anticipated perpendicular-like appearance nor a clear origin.

The energy level structure of both the $\tilde{B}\,^2E$ and $\tilde{X}\,^2A_1$ states of the metal monoborohydrides closely resembles that of the corresponding monomethyls.[5,31,32] These energy levels can be described by considering two factors. First, the borohydrides are prolate symmetric top molecules belonging to the C_{3v} symmetry group. Therefore, their rotational energy level structure is split into various sublevels, labeled by $K(=K_R+\zeta_e)$, where K_R and ζ_e are the projections of the rotational angular momentum of the nuclei (**R**) and the electronic orbital angular momentum (**L**) onto the symmetry axis, respectively. Second, the spin angular momentum associated with the unpaired electron (**S**) must also be taken into account. In the ground $^2A_1$ state, the spin of the unpaired electron interacts with the rotational angular momentum of the molecule to split each rotational level into two spin-rotation components, labeled by J, the total angular momentum. These two components are identified by F_1 (e parity) and F_2 (f parity). In the ^2E state, the spin of the unpaired electron interacts with the electronic orbital angular momentum and gives rise to the $^2E_{1/2}(F_1)$ and $^2E_{3/2}(F_2)$ spin-orbit components. Each rotational level in each spin-orbit component is further split into e and f parity levels by the spin-rotation and Jahn-Teller interactions. This splitting is similar to Λ-type doubling in a linear molecule[41] and, as noted by both Hougen[41] and Brown,[42] should be most predominant in the $K'=1$ levels and may be negligible in the other observed K' levels. A more detailed description of the energy level structure along with energy level diagrams for ^2E and $^2A_1$ states can be found in Refs. 5, 31, and 32

The allowed rotational transitions between the $\tilde{B}\,^2E$ and $\tilde{X}\,^2A_1$ states are determined by the selection rules for a perpendicular-type transition, $\Delta K=\pm 1$ and $\Delta J=0,\pm 1$. Including parity dependence,[43] this results in six branches per ΔK subband within each spin-orbit component. Each individual branch is labeled by the notation ${}^{\Delta K}\Delta J_{F_i' F_j''}$ $(i=1,2;j=1,2)$, where ΔK is represented by a lower case $p(\Delta K=-1)$ or $r(\Delta K=+1)$.[42] Because the rotation of the borohydrides about the symmetry axis exchanges the protons of the BH_4^- ligand, the effect of nuclear spin statistics must also be considered. In this case, this phenomenon gives rise to two nuclear spin states: ortho ($K=3N$, where N is an in-

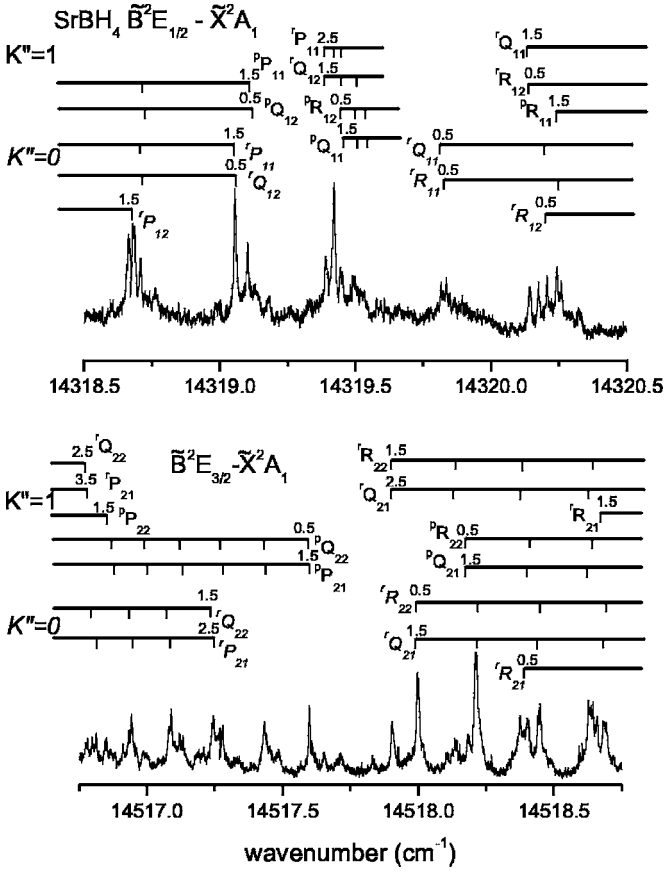

FIG. 3. Subsections of the high resolution spectra of the $\tilde{B}\,^2E_{1/2}$-$\tilde{X}\,^2A_1$ (top panel) and the $\tilde{B}\,^2E_{3/2}$-$\tilde{X}\,^2A_1$ (bottom panel) spin-orbit components of $SrBH_4$. For each component, 15 of the 18 possible branches are shown. In each spectrum, branches assigned to the $K'=1\leftarrow K''=0$ subband are labeled on the bottom in italics and those belonging to the $K'=2\leftarrow K''=1$ and $K'=0\leftarrow K''=1$ subbands are labeled on the top. Individual rotational lines are labeled by the notation $^{\Delta K}\Delta J_{F_i'F_j''}(i=1,2;j=1,2)$. In the $\tilde{B}\,^2E_{1/2}$-$\tilde{X}\,^2A_1$ spin-orbit component (top panel) the rotational lines of 11 of the 15 observed branches are spaced by $\sim 2B$ and the $^rP_{11}$, $^rQ_{12}$, $^pR_{12}$, and $^pQ_{11}$ branches have almost converged near the origin.

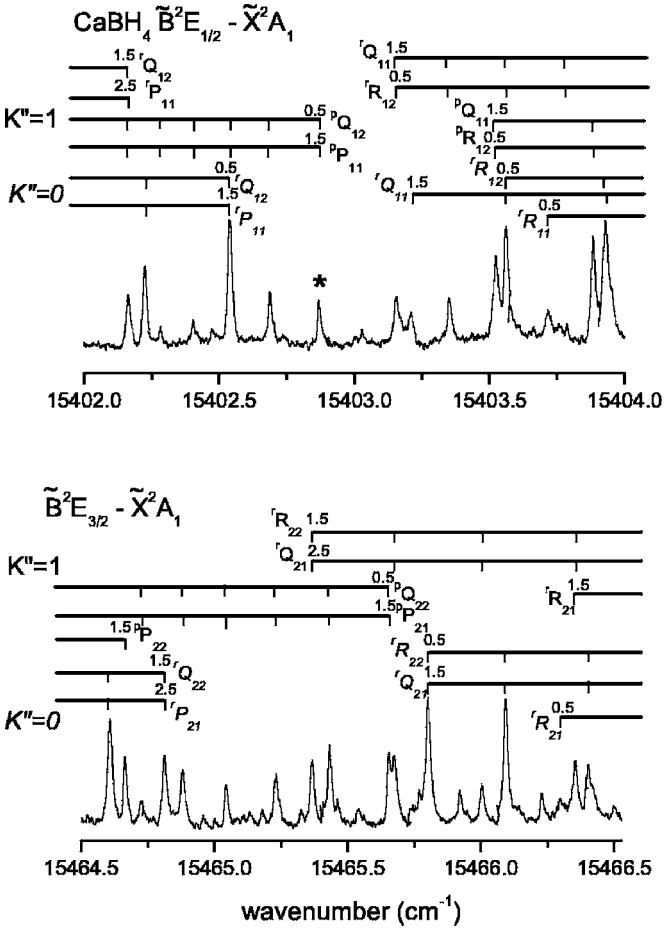

FIG. 4. A portion of the high resolution spectra, including rotational assignments, for each spin-orbit component of the $\tilde{B}\,^2E_{1/2}$-$\tilde{X}\,^2A_1$ transition of $CaBH_4$. Again, the $K'=1\leftarrow K''=0$ (on the bottom in italics), $K'=2\leftarrow K''=1$, and $K'=0\leftarrow K''=1$ (on the top) subbands are shown, and individual rotational lines are labeled by $^{\Delta K}\Delta J_{F_i'F_j''}(i=1,2;j=1,2)$. For the $\tilde{B}\,^2E_{3/2}$-$\tilde{X}\,^2A_1$ spin-orbit component (bottom panel), the $^pQ_{22}$ and $^pP_{21}$ branches begin at the blue of the $^rQ_{21}$ and $^rR_{22}$ branches, resulting in a very overlapped and congested structure for this spin-orbit component. The $\tilde{B}\,^2E_{1/2}$-$\tilde{X}\,^2A_1$ spin-orbit component (top panel) has a clear origin; however, the $^pP_{11}$ branch can only be ambiguously assigned, suggesting a perturbation (see text).

teger) and para ($K\neq 3N$).[43] Molecules in each of these nuclear spin states behave like separate species and cannot rotationally cool to one another in the free jet expansion. As a result, both $K''=0$ and $K''=1$ levels are populated in the jet. Therefore, according to the selection rule $\Delta K=\pm 1$, three ΔK subbands should be predominantly observed in our spectra, $K'=1\leftarrow K''=0$, $K'=0\leftarrow K''=1$, and $K'=2\leftarrow K''=1$, which give rise to 36 branches in total.

Rotational assignments of the $\tilde{B}\,^2E$-$\tilde{X}\,^2A_1$ transition of $SrBH_4$ were completed by first examining the $\tilde{B}\,^2E_{3/2}$-$\tilde{X}\,^2A_1$ spin-orbit component. The similar appearance of this component with the $\tilde{A}\,^2E_{3/2}$-$\tilde{X}\,^2A_1$ transition of $SrCH_3$[5] facilitated branch assignments. Because no previous ground state combination differences were available, rotational assignments were made within each ΔK subband using first lines and then generated lower state combination differences. Subsequently, this set of combination differences was used to make rotational assignments in the $\tilde{B}\,^2E_{1/2}$-$\tilde{X}\,^2A_1$ component, which lacked any similarity with the corresponding component of $SrCH_3$. In this case, a series of branches on each side of the origin were first identified and then grouped together utilizing the combination differences. Using this method, 17 of the 18 possible branches from all three observed ΔK subbands were identified in this spin-orbit component. Figure 3 shows a portion of the spectra with line assignments $[^{\Delta K}\Delta J_{F_i'F_j''}(i=1,2;j=1,2)]$, for each spin-orbit component of the $\tilde{B}\,^2E$-$\tilde{X}\,^2A_1$ transition of $SrBH_4$. The unusual structure of the $\tilde{B}\,^2E_{1/2}$-$\tilde{X}\,^2A_1$ component, as compared to the $\tilde{B}\,^2E_{3/2}$-$\tilde{X}\,^2A_1$ spin-orbit component, can clearly be observed in the four branches ($^rP_{11}$, $^rQ_{12}$, $^pR_{12}$, and $^pQ_{11}$) that have converged near the origin and have adopted an appearance similar to a strong Q branch.

The assignment of the $\tilde{B}\,^2E$-$\tilde{X}\,^2A_1$ transition of $CaBH_4$ was not as straightforward. Unfortunately, neither spin-orbit component exhibited the expected appearance of a perpendicular transition, and both were exceptionally congested. In addition, each component lacked a clear origin, making it difficult to identify the starting position of any branch. As a

result, a different approach was utilized in order to make the rotational assignments. Again, as with $SrBH_4$, a set of lower state combination differences was not available from previous spectroscopic work. However, in the analysis of the $\tilde{B}\,^2E$-$\tilde{X}\,^2A_1$ transition of $SrBH_4$, the lower state combination differences were found to be consistently ~1.02 times smaller then the analogous combination differences for $SrCH_3$.[44] Therefore, initially, this factor was applied to the lower state combination differences of $CaCH_3$[45] in order to generate an approximate set of combination differences for $CaBH_4$, which were then used to make rotational assignments for all of the possible R and P branches in the $\tilde{B}\,^2E_{3/2}$-$\tilde{X}\,^2A_1$ spin-orbit component. As was the case for $SrBH_4$, the lower state combination differences from this component were then applied to the $\tilde{B}\,^2E_{1/2}$-$\tilde{X}\,^2A_1$ spin-orbit component of $CaBH_4$. Using this method, 10 of the 12 possible R and P branches for this spin-orbit component were identified. The two branches that were not observed ($^rP_{12}$ and $^pR_{11}$) form combination difference pairs with the $^rR_{12}$ and $^pP_{11}$ branches, respectively. As a result the J assignments of the $^rR_{12}$ and $^pP_{11}$ branches were made by identifying their first lines. All 12 possible Q branches, from both spin-orbit components, were also assigned. However, the majority of these branches were not completely resolved from their associated P or R branch, suggesting that the ground state spin-rotation interaction is quite small. Figure 4 shows a portion of the high resolution spectra with rotational assignments $[^{\Delta K}\Delta J_{F_i' F_j''}(i=1,2;j=1,2)]$ for each spin-orbit component of this electronic transition. In the top spectrum, the starting positions of the branches of the $\tilde{B}\,^2E_{3/2}$-$\tilde{X}\,^2A_1$ component can be observed to vary greatly from those of $SrBH_4$. For example, the $^pP_{21}$ branch begins at the blue of the $^rR_{22}$ branch, which obscures the origin of the $\tilde{B}\,^2E_{3/2}$-$\tilde{X}\,^2A_1$ spin-orbit component. This irregular pattern contributed to the difficulty in identifying the starting positions for each series of lines.

IV. ANALYSIS

The $\tilde{B}\,^2E$-$\tilde{X}\,^2A_1$ transitions of $SrBH_4$ and $CaBH_4$ were modeled using a symmetric top effective Hamiltonian[41,42,46] that incorporated the rotation of the molecule, along with centrifugal distortion corrections, and the spin-rotation, spin-orbit, Jahn-Teller, and Coriolis interactions. Using the matrix elements of Endo *et al.*,[46] in a Hund's case (a) basis, this Hamiltonian was incorporated into a computer program, and a least squares fit of the measured data was performed.

For $SrBH_4$, 181 lines from 35 of the 36 possible branches from all three observed ΔK subbands were included in the fit. Clearly resolved lines were weighted according to the experimental uncertainty (0.004 cm^{-1}), while overlapped lines were deweighted slightly (0.008 cm^{-1}). The measured lines can be found in Ref. 47. In the ground state only one rotation (B) and one spin-rotation $[\varepsilon_{bc}=(\varepsilon_{bb}+\varepsilon_{cc})/2]$ constant were allowed to vary. The A rotational constant in the ground state could not be determined from the current data set because no $\Delta K=0$ transitions were observed. As a result, it was fixed to the theoretical value given by Chan and Hamilton.[34] Additionally, no centrifugal distortion terms were found to be necessary due to the low J values ($J''<9.5$) observed in the spectra. For the excited state, a set of molecular constants similar to those used to describe the $\tilde{A}\,^2E$ state of $SrCH_3$[5] were employed. These included rotation (A,B), spin-orbit ($a\zeta_e d, a_D\zeta_e d$), Coriolis ($A\zeta_t$), and spin-rotation ($\varepsilon_{aa},\varepsilon_1$) terms. The spectroscopic parameters of the $\tilde{B}\,^2E$ and $\tilde{X}\,^2A_1$ states of $SrBH_4$ derived from the final fit are listed in Table I along with those of the $\tilde{A}\,^2E$ and $\tilde{X}\,^2A_1$ states of $SrCH_3$ for comparison.

The fitting of the $\tilde{B}\,^2E$-$\tilde{X}\,^2A_1$ transition data of $CaBH_4$ was not as straightforward as it was for $SrBH_4$. In the first attempt at fitting the rotational transitions of the three observed ΔK subbands, residuals for the $^pP_{11}$ branch were found to be unusually large. As a result, a second fit was

TABLE I. Spectroscopic constants (in cm^{-1}) for the $\tilde{A}\,^2E$ and $\tilde{X}\,^2A_1$ states of $SrCH_3$ and the $\tilde{B}\,^2E$ and $\tilde{X}\,^2A_1$ states of $SrBH_4$.

	$SrCH_3$[b]		$SrBH_4$	
Constant[a]	$\tilde{X}\,^2A_1$	$\tilde{A}\,^2E$	$\tilde{X}\,^2A_1$	$\tilde{B}\,^2E$
T	0.0	13 800.3762(9)	0.0	14 422.5566(18)
$a\zeta_e d$		279.1651(17)		198.4994(36)
$a_D\zeta_e d$		−0.0297(15)		−0.0337(15)
$A\zeta_t$		5.248 33(83)		4.0123(11)
A	5.390[c]	5.334 94(75)	4.213[c]	4.177 08(76)
B	0.193 833 336(16)	0.195 068(21)	0.188 367(50)	0.194 290(44)
D_N	$2.148\,93(11)\times10^{-7}$			
D_{NK}	$1.613\,49(51)\times10^{-5}$			
H_{NK}	$2.920(21)\times10^{-10}$			
H_{KN}	$3.18(43)\times10^{-9}$			
ε_{aa}	0.000 883(34)	0.3692(33)		0.0792(44)
ε_{bc}	0.004 128 52(43)		0.002 62(39)	
ε_1		−0.094 15(12)		0.185 09(16)

[a]Values in parentheses are 1σ standard deviations, in units of the last significant digits.
[b]From Ref. 5
[c]Fixed to the theoretical value (Ref. 34).

TABLE II. Spectroscopic constants (in cm^{-1}) for the $\tilde{A}\,^2E$ and $\tilde{X}\,^2A_1$ states of $CaCH_3$ and the $\tilde{B}\,^2E$ and $\tilde{X}\,^2A_1$ states of $CaBH_4$.

	$CaCH_3$[b]		$CaBH_4$[c]		$CaBH_4$[d]	
Constant[a]	$\tilde{X}\,^2A_1$	$\tilde{A}\,^2E$	$\tilde{X}\,^2A_1$	$\tilde{B}\,^2E$	$\tilde{X}\,^2A_1$	$\tilde{B}\,^2E$
T	0.0	14 743.3822(11)	0.0	15 438.3932 (62)	0.0	15 438.3936(19)
$a\zeta_e d$		72.7092(18)		62.9654(11)		62.9646(34)
$a_D\zeta_e d$		-8.86×10^{-4}				
$A\zeta_t$		5.3600(3)		4.126 69(49)		4.1272(12)
A	5.448 31	5.3855(6)	4.230[e]	4.185 96(44)	4.230[e]	4.186 37(65)
B	0.252 384 7	0.254 270(7)	0.247 357(30)	0.255 106(26)	0.247 367(31)	0.255 127(30)
D_K	7.03×10^{-5}	6.437×10^{-5}				
D_N	$3.544\,852\times10^{-7}$	3.6203×10^{-7}				
D_{NK}	$1.995\,314\times10^{-5}$	1.2980×10^{-5}				
$\eta_e\xi_t$		3.522×10^{-5}				
ε_{aa}		0.0129(17)		−0.0480(11)		−0.0477(30)
ε_{bc}	0.001 851 05	0.0196(17)				
ε_1		−0.0251(1)		0.086 045(81)		0.086 18(10)

[a]Values in parentheses are 1σ standard deviations, in units of the last significant digits.
[b]From Ref. 32.
[c]Fit included 34 of the 36 possible branches for the $\tilde{B}\,^2E$-$\tilde{X}\,^2A_1$ transition. The $^pP_{11}$ branch is labeled such that one line remains unassigned.
[d]Fit included all of the possible branches for the $\tilde{B}\,^2E_{3/2}$-$\tilde{X}\,^2A_1$ spin-orbit component and all of the observed branches for the 1-0 and 2-1 subbands of the $\tilde{B}\,^2E_{1/2}$-$\tilde{X}\,^2A_1$ spin-orbit component. No lines from the 0-1 subband of the $\tilde{B}\,^2E_{1/2}$-$\tilde{X}\,^2A_1$ spin-orbit component were included.
[e]Fixed to the theoretical value (Ref. 34).

conducted without this branch. A subsequent prediction, using the parameters of this fit, indicated that the J values of the $^pP_{11}$ branch should be decreased by 1 from the original assignment. Initially, this result was not surprising as this branch was originally assigned by the identification of a supposed first line. However, these new J assignments of the $^pP_{11}$ branch resulted in one line [identified with an asterisk (*) in Fig. 4] being unassigned. Subsequent attempts to ascertain the identity of this line in the context of this fit were unsuccessful. The iodine calibration spectrum and etalon trace signal were examined closely to ensure that this line was a real feature and not the result of a laser mode hop. In addition, attempts at reassigning the observed branches of all three ΔK subbands in the $\tilde{B}\,^2E_{1/2}$-$\tilde{X}\,^2A_1$ spin-orbit component to include this line were unsuccessful. The line positions of the $^pP_{11}$ branch were also calculated using the lower state combination differences from the 2-1 subband to determine the $K''=1$ rotational level energies, and the upper state ($K'=0$) rotational level energies were calculated from upper state combination differences of the $^pR_{12}$ and $^pP_{12}$ branches (assuming that the e and f parity splitting in the $K'=0$ levels were negligible as they were for $CaCH_3$,[31,32] $SrCH_3$,[5] and $SrBH_4$). This calculation showed that the new J assignments for the $^pP_{11}$ branch with one line left unassigned were plausible.

Using these rotational line assignments, 169 lines from 34 of the 36 possible branches were included in the fit and are listed in Ref. 47. As with $SrBH_4$, clearly resolved ($0.004\ cm^{-1}$) and overlapped lines ($0.008\ cm^{-1}$) were weighted differently. In the ground state only the rotational constant, B, was allowed to vary. As with $SrBH_4$, no $\Delta K=0$ transitions were observed; therefore, the A rotational constant in the ground state could not be determined and was fixed to the theoretical value.[34] As mentioned previously, the spin-rotation splitting in the $\tilde{X}\,^2A_1$ state appeared unresolved; thus, ε_{bc} was fixed to zero. In the upper state, the rotation (A,B), spin-orbit ($a\zeta_e d$), Coriolis ($A\zeta_t$), and spin-rotation ($\varepsilon_{aa},\varepsilon_1$) terms were included in the fit. Unlike for $SrBH_4$, it was found that the $a_D\zeta_e d$ term could not be determined for $CaBH_4$. The spectroscopic parameters of the $\tilde{B}\,^2E$ and $\tilde{X}\,^2A_1$ states of $CaBH_4$ determined from this fit are listed in Table II along with those of the $\tilde{A}\,^2E$ and $\tilde{X}\,^2A_1$ states of $CaCH_3$ for comparison.

One likely explanation for the identity of the unassigned line in the $\tilde{B}\,^2E_{1/2}$-$\tilde{X}\,^2A_1$ spin-orbit component is that it is indeed the first line of the $^pP_{11}$ branch. This would suggest that the rotational energy levels of the $K'=0$ state of the $\tilde{B}\,^2E_{1/2}$ spin-orbit component are being perturbed by some nearby electronic state. For $CaCH_3$, the $K'=1$ level of the $\tilde{B}\,^2A_1$ state was found to be perturbed by a vibrational level of the $\tilde{A}\,^2E$ state. A similar scenario is possible for $CaBH_4$, in which a vibronic level of the $\tilde{A}\,^2A_1$ state interacts with the $K'=0$ state of the $\tilde{B}\,^2E_{1/2}$ spin-orbit component. As a result, an alternative fit of the $\tilde{B}\,^2E$-$\tilde{X}\,^2A_1$ transition data of $CaBH_4$, in which the data from the 0-1 subband of the $\tilde{B}\,^2E_{1/2}$-$\tilde{X}\,^2A_1$ spin-orbit component were removed, was performed. This alternative fit included both spin-orbit components of the 1-0 and 2-1 subbands and only the 0-1 subband of the $\tilde{B}\,^2B_{3/2}$-$\tilde{X}\,^2A_1$ component. In this fit, the rotation (A,B), spin-orbit ($a\zeta_e d$), Coriolis ($A\zeta_t$), and spin-rotation ($\varepsilon_1,\varepsilon_{aa}$) parameters were determined and are also included in Table II for comparison.

TABLE III. Metal—ligand separations for the borohydrides and monomethyls of calcium and strontium.

State	M-L separation	$CaBH_4$[a]	$CaBH_4$	$CaCH_3$[b]
$\tilde{X}\,^2A_1$	r_{Ca-L} (Å)	2.415	2.414,[c] 2.430[d]	2.348
^2E	r_{Ca-L} (Å)	2.376		2.342
		$SrBH_4$[a]	$SrBH_4$	$SrCH_3$[e]
$\tilde{X}\,^2A_1$	r_{Sr-L} (Å)	2.574	2.596[c]	2.487
^2E	r_{Sr-L} (Å)	2.532		2.481

[a]Calculated from the rotational constant, B, from the current investigation and fixing the BH_4^- ligand geometry to that of Ref. 34.
[b]Experimental data from Ref. 6.
[c]Theoretical data from Ref. 34.
[d]Theoretical data from Ref. 33.
[e]Experimental data from Ref. 5.

V. DISCUSSION

A. Geometry

Because rotational constants for only one isotopolog of both $CaBH_4$ and $SrBH_4$ were determined in this study, it is difficult to ascertain the structural parameters of these molecules. One approach that can be employed to extract structural information from the observed rotational constants is to fix the geometry of the BH_4^- ligand to that calculated for the ground state by Chan and Hamilton[34] and assume that the ligand structure is invariant upon promotion from the $\tilde{X}\,^2A_1$ to $\tilde{B}\,^2E$ state. Using this method, the rotational constant, B, can be used to derive the metal-boron separation. The calculated distances are listed in Table III along with the theoretical values[33,34] for comparison. For the ground states, there is a very good agreement (less than 1% difference) between the metal-boron separations obtained in this work and those calculated by Chan and Hamilton.[34] The agreement is slightly worse for the calculations of Ortiz.[33] For the excited states no theoretical predictions of the rotational constants exist; therefore, no direct comparison of the experimental metal-boron separations to the theoretical values can be made.

Using these experimental values of the metal-ligand separation, the change in this separation from the $\tilde{X}\,^2A_1$ to $\tilde{B}\,^2E$ state can be examined. For $CaBH_4$ and $SrBH_4$, the metal-ligand separations decrease by factors of 0.9834 (0.040 Å) and 0.9837 (0.042 Å), respectively. This is in contrast to the metal-ligand separation in $CaCH_3$ and $SrCH_3$, where from the $\tilde{X}\,^2A_1$ to $\tilde{A}\,^2E$ states the metal-carbon distances (Table III) decreased by factors of only 0.9963 (0.006 Å) and 0.9968 (0.006 Å), respectively. The larger decrease in the metal-ligand separation for the metal borohydrides, as compared to the metal monomethyls, is consistent with the theoretical calculations of Ortiz[33] for $CaBH_4$. In this work, the metal-boron separation in the first excited ^2E state was found to decrease by a factor of 0.9794 (0.05 Å) as compared to the ground state. This larger change in the metal-ligand separation was attributed to an increased amount of d atomic orbital character in the first excited ^2E state of $CaBH_4$ as compared to $CaCH_3$. For calcium and strontium-containing molecules, the first two excited states are derived predominantly from p and d atomic orbitals located on the metal atom. For example, the orbital character of the $\tilde{A}\,^2\Pi$ state of SrOH[48] is 92% comprised of contributions from the $5p\pi$ and $4d\pi$ atomic orbitals on the strontium ion. The molecular parameters in these states are often a reflection of the ratio of p and d atomic orbital characters in the state. In the case of $CaBH_4$, Ortiz suggested that the increased d orbital character would result in the unpaired electron residing in a more diffuse orbital, which, in turn, allows the BH_4^- ligand to more closely approach the Ca^+ cation. Similar calculations for $SrBH_4$ do not exist, but, as mentioned previously, a similar change between the ground and excited state rotational constants was observed. This may imply that an increased amount of d character is also present in the $\tilde{B}\,^2E$ state of $SrBH_4$ as compared to $SrCH_3$.

Finally, fluxional behavior, in which the BH_4^- ligand undergoes internal rotation, was predicted to have a low-energy barrier in the alkali metal borohydrides. However, a splitting of rotational lines inherent with the internal rotation of the BH_4^- ligand[29] was not resolved in the $\tilde{B}\,^2E$-$\tilde{X}\,^2A_1$ transitions of $CaBH_4$ and $SrBH_4$. This indicates that the barrier to this internal motion is high in the borohydrides of calcium and strontium, as it is in $NaBH_4$[9] and $LiBH_4$.[14]

B. Jahn-Teller and fine structure interactions

For both $CaBH_4$ and $SrBH_4$ the orbitally degenerate $\tilde{B}\,^2E$ state may be subject to Jahn-Teller coupling. However, electronic states that exhibit a large spin-orbit interaction are expected to exhibit a small Jahn-Teller splitting.[49] Additionally, electronic states arising predominantly from atomic orbitals located on the metal atom, such as the $\tilde{B}\,^2E$ states of the metal borohydrides, should have reduced Jahn-Teller coupling. This is a result of the hydrogen atoms of the ligand being located far from the metal atom, which causes the coupling of degenerate vibrational and electronic wave functions to be small.[50]

Assuming that the Jahn-Teller coupling is small in the $\tilde{B}\,^2E$ states of $CaBH_4$ and $SrBH_4$, the projections of the electronic (ζ_e) and vibronic (ζ_t) angular momenta on the symmetry axis can be calculated for these states. First, ζ_t can be calculated from the ratio of $A\zeta_t$ to A for the $\tilde{B}\,^2E$ state of each molecule ($CaBH_4$ ζ_t=0.9859; $SrBH_4$ ζ_t=0.9606). Next, these values of ζ_t can be used to calculate ζ_e via the following equation:[51]

$$\zeta_t = \zeta_e d + \frac{1-d}{2}\zeta_2, \tag{1}$$

in which d is the Jahn-Teller quenching parameter ($1>|d|>0$) and ζ_2 is the vibrational Coriolis coupling coefficient for the Jahn-Teller active degenerate vibrational mode. If the Jahn-Teller effect is neglected (d=1), then according to Eq. (1), $\zeta_e=\zeta_t$ and hence ζ_e=0.9859 and 0.9606 for $CaBH_4$ and $SrBH_4$, respectively. For an electronic state derived primarily from a p atomic orbital, ζ_e should be close to 1. Any reduction in this value can be attributed to an increase in the amount of atomic orbital character other then p. Although these values of ζ_e indicate that the $\tilde{B}\,^2E$ states of $CaBH_4$ and $SrBH_4$ arise predominantly from p orbitals located on the

metal, a comparison with the ζ_e values of $CaCH_3$ (0.9953)[31] and $SrCH_3$ (0.9838)[5] shows that they are reduced slightly for the borohydrides. This suggests that the $\tilde{B}\,^2E$ states of $CaBH_4$ and $SrBH_4$ contain less p orbital character than the $\tilde{A}\,^2E$ states of the corresponding monomethyls.

A final indication of the reduction of the amount of p orbital character in $\tilde{B}\,^2E$ states of $CaBH_4$ and $SrBH_4$ as compared to the $\tilde{A}\,^2E$ states of $CaCH_3$ and $SrCH_3$ can be found by examining the spin-orbit interaction. The energy separation of the two spin-orbit components of the $\tilde{B}\,^2E$ states is given by $a\zeta_e d$, where a describes the magnitude of the spin-orbit splitting. A value of a may be calculated using the expression $a\zeta_e d = a\zeta_t$, assuming that the Jahn-Teller interaction may be neglected. For $SrBH_4$ ($a\zeta_e d = 198.4994\ cm^{-1}$), the magnitude of the spin-orbit coupling constant is estimated to be $a = 206.6411\ cm^{-1}$. This value is 27% smaller as compared to $SrCH_3$ ($a = 283.772\ cm^{-1}$).[5] This reduction may be rationalized by considering the atomic orbital contributions to the spin-orbit splitting parameter for the first excited ^2E states of either $SrCH_3$ or $SrBH_4$, which are given by the equation

$$a = c_{5p\pi}^2 \zeta_{5p} + c_{4d\pi}^2 \zeta_{4d} + c_{n\ell}^2 \zeta_{n\ell}, \tag{2}$$

where $c_{5p\pi}$, $c_{4d\pi}$, and $c_{n\ell}$ are expansion coefficients and ζ_{5p}, ζ_{4d}, and $\zeta_{n\ell}$ are the atomic spin-orbit coupling parameters.[52] This equation can be further simplified by removing the contributions from atomic orbitals other than $5p\pi$ and $4d\pi$ to give

$$a = c_{5p\pi}^2 \zeta_{5p} + c_{4d\pi}^2 \zeta_{4d}. \tag{3}$$

This is a relatively safe assumption because, as mentioned earlier, in the case of SrOH[48] the $5p\pi$ and $4d\pi$ orbitals comprise 92% of the orbital character of the $\tilde{A}\,^2\Pi$ state. For strontium, the atomic spin-orbit coupling parameter is larger for the $5p$ orbital ($\zeta_{5p} = 534\ cm^{-1}$) than it is for the $4d$ orbital ($\zeta_{4d} = 112\ cm^{-1}$).[53] Thus, if the amount of the $5p$ character decreases and the amount of $4d$ character increases, the molecular spin-orbit coupling constant is reduced. This change in the amount of d character most likely accounts for the majority of the 27% reduction in the magnitude of the molecular spin-orbit coupling constant in $SrBH_4$ as compared to $SrCH_3$.

A similar reduction in the molecular spin-orbit coupling parameter, a, in the first excited ^2E state is observed for $CaBH_4$ ($a = 63.87\ cm^{-1}$) as compared to $CaCH_3$ ($a = 72.7092\ cm^{-1}$).[32] In this case the spin-orbit coupling constant may be calculated according to the equation

$$a = c_{4p\pi}^2 \zeta_{4p} + c_{3d\pi}^2 \zeta_{3d}. \tag{4}$$

For calcium, the atomic spin-orbit coupling parameter is again larger for the p orbital ($\zeta_{4p} = 148\ cm^{-1}$) than for the d orbital ($\zeta_{3d} = 24\ cm^{-1}$),[54] but the difference in magnitude is not as great as for strontium. The reduction in a can again most likely be largely attributed to an increase in the amount of d character in the $\tilde{B}\,^2E$ state of $CaBH_4$ as compared to the $\tilde{A}\,^2E$ state of $CaCH_3$.

Another interesting comparison that can be made between the monomethyls and borohydrides of strontium and calcium involves the spin-rotation constant ε_1. Using the pure precession relationship and unique perturber approximation, the following expression for ε_1 has been derived:[31,44]

$$\varepsilon_1 = \frac{aB\ell(\ell+1)}{E_{^2E} - E_{^2A_1}}, \tag{5}$$

where ℓ is the atomic orbital angular momentum and E is the state energy. This equation shows that ε_1 arises from an interaction of a ^2E state with a neighboring $^2A_1$ state. This is analogous to the Λ-doubling constant, p, in a $^2\Pi$ state, which accounts for its interaction with a neighboring $^2\Sigma^+$ state. According to Eq. (5), the sign of ε_1 should be dependent on the relative energy positioning of the ^2E and $^2A_1$ states. For example, if the ^2E state lies higher in energy then the $^2A_1$ state, then ε_1 will have a positive sign. For both $CaBH_4$ ($0.086\,18\ cm^{-1}$) and $SrBH_4$ ($0.185\,09\ cm^{-1}$) the sign of ε_1 has changed in comparison with $CaCH_3$ ($-0.0251\ cm^{-1}$)[32] and $SrCH_3$ ($-0.094\,15\ cm^{-1}$).[5] This is further evidence that the first excited ^2E and $^2A_1$ states in the borohydrides have reordered in energy as compared with the monomethyls.[25]

For both $CaBH_4$ and $SrBH_4$ the magnitude of ε_1 has increased in comparison with the monomethyls. As both a and B have decreased for $CaBH_4$ and $SrBH_4$, this increase in magnitude is a reflection of the first excited ^2E and $^2A_1$ states lying closer in energy for the borohydrides. In the $\tilde{B}\,^2E$ state of $SrBH_4$, the magnitude of ε_1 is nearly equal to the rotational constant, B ($0.194\,290\ cm^{-1}$). As mentioned previously, ε_1 is analogous to the Λ-doubling constant, p, and the two parameters can be related by the expression $\varepsilon_1 = p/2$.[41] Kopp and Hougen[55] have shown that if p equals approximately twice the B value in a $^2\Pi_{1/2}$ state, the energy level structure of this state becomes very similar to that of a $^2\Sigma^+$ state. Applying these arguments to a $^2E_{1/2}$ state, if ε_1 equals approximately B, then the energy level structure of this state will appear like a $^2A_1$ state. This is precisely what has been observed in the $\tilde{B}\,^2E_{1/2}$ spin-orbit component of $SrBH_4$ and explains the unique structure of this component, in which each branch is spaced by $\sim 2B$. A similar structure is not seen in the $\tilde{B}\,^2E_{1/2}$-$\tilde{X}\,^2A_1$ spin-orbit component of $CaBH_4$, as ε_1 has increased but is not quite equal in magnitude to B. Therefore, $\sim 1B$ and $\sim 3B$ spaced branches are still observed in this spin-orbit component.

Finally, it is of interest to compare the experimentally determined values of ε_1 with those derived from Eq. (5). For $SrBH_4$ the values $a = 206.6411\ cm^{-1}$, $B = 0.194\,290\ cm^{-1}$, $E(\tilde{B}\,^2E) = 14\,422.5566\ cm^{-1}$, and $E(\tilde{A}\,^2A_1) = 13\,685\ cm^{-1}$ were used. Assuming that the $\tilde{B}\,^2E$ state arises solely from a p atomic orbital ($\ell = 1$), ε_1 was estimated to be $0.1089\ cm^{-1}$. For $CaBH_4$ ($a = 63.87\ cm^{-1}$, $B = 0.255\,127\ cm^{-1}$, $E(\tilde{B}\,^2E) = 15\,438.3936\ cm^{-1}$, $E(\tilde{A}\,^2A_1) = 14\,800\ cm^{-1}$, and $\ell = 1$) a similar calculation estimated ε_1 to be $0.051\ cm^{-1}$. For each molecule the calculated value is approximately 40% smaller than the experimentally determined parameter, consistent with $\ell > 1$ and the additional d orbital character. However, some of these differences may be attributed to the approxi-

mations made in deriving Eq. (5). Similar calculations of ε_1 in the $\tilde{A}\,^2E$ state of $CaCH_3$[31] and $SrCH_3$[5] found differences between the calculated and experimentally determined parameters of only about 20%. This better agreement for the monomethyls as compared to the borohydrides is consistent with more p atomic orbital character (ℓ closer to 1) in the $\tilde{A}\,^2E$ state of the monomethyls as compared to the $\tilde{B}\,^2E$ state of the borohydrides.

The remaining experimentally determined spin-rotation constant (ε_{aa}) can also be estimated using the unique perturber approximation and pure precession relationship,[56]

$$\varepsilon_{aa} = -\frac{4a\zeta_e dA\zeta_t}{E_{\tilde{B}\,^2E} - E_{\text{Higher lying }^2E}}. \tag{6}$$

According to the above equation, ε_{aa} should be positive for the $\tilde{B}\,^2E$ states of $SrBH_4$ and $CaBH_4$. A value of $0.0792\ \text{cm}^{-1}$ was determined for ε_{aa} in the $\tilde{B}\,^2E$ state of $SrBH_4$. Unfortunately, this parameter cannot be quantitatively estimated using Eq. (6) as no information exists for any of the other excited ^2E states of $SrBH_4$. However, qualitatively, this equation does indicate that ε_{aa} should be small and positive as the neighboring ^2E states should be higher in energy than the $\tilde{B}\,^2E$ state of $SrBH_4$. Interestingly, a similar qualitative agreement was not found for ε_{aa} in the $\tilde{B}\,^2E$ state of $CaBH_4$. Here, this constant ($\varepsilon_{aa}=-0.0477\ \text{cm}^{-1}$) was found to be small and negative in disagreement with Eq. (6). However, ε_{aa} was only marginally determined in both fits of $CaBH_4$, making its true physical significance somewhat dubious.

C. Perturbation in the $\tilde{B}\,^2E_{1/2}$ state of $CaBH_4$

One possible explanation for the negative value of ε_{aa} for $CaBH_4$ is that it is a result of a perturbation to the $\tilde{B}\,^2E_{1/2}$ spin-orbit component. For $CaCH_3$,[6] the $\tilde{B}\,^2A_1$ state was found to be perturbed. In this case, the $K'=1$ energy levels were affected by an interaction with an excited $\tilde{A}\,^2E$ vibrational state. This perturbation caused the energy levels of the F_1 spin-rotation component to be higher in energy than those of the F_2 component, contrary to the $K'=0$ energy level. As a result, the $K'=1$ sublevel data could not be included in the final fit. A similar interaction is possible, in reverse, in $CaBH_4$ where the $\tilde{B}\,^2E$ state interacts with an excited vibrational level of the $\tilde{A}\,^2A_1$ state. The ambiguous J assignments of the rotational lines of the $^pP_{11}$ branch in the 0–1 subband of the $\tilde{B}\,^2E_{1/2}$-$\tilde{X}\,^2A_1$ spin-orbit component suggest that the $K'=0$ rotational levels of this spin-orbit component are perturbed. More specifically, the $^pP_{11}$ branch terminates in levels with e parity, which suggests that these levels are the most affected by the perturbation. This is further supported by the assignment of the $^pP_{12}$ and $^pR_{12}$ branches without complication, suggesting that the f levels of the $K'=0$ state of the $\tilde{B}\,^2E_{1/2}$ spin-orbit component are relatively unaffected by the perturbation. This scenario where the e and f parity levels are affected differently by the perturbation is possible as long as the parity splitting in the perturbing state is large and the e level interaction is more in resonance than the f level interaction. From the pure precession and unique perturber approximations,[51] it is known that the parity splitting in the $\tilde{A}\,^2A_1$ should be similar to that of the $\tilde{B}\,^2E_{1/2}$ spin-orbit component. In this component the splitting is described by ε_1, and, as outlined previously, the magnitude of this parameter has increased significantly in comparison with $CaCH_3$. This increase in magnitude could result in the perturbation dominating the e levels of the $K'=0$ sublevel of the $\tilde{B}\,^2E_{1/2}$ spin-orbit component. However, when the $K'=0$ data were removed from the fit, a negative value of ε_{aa} was still found, further suggesting that the $K'=1$ and 2 levels may also be affected, although less severely. Unfortunately, it is difficult to determine which of the vibrational levels of the $\tilde{A}\,^2A_1$ state is causing the perturbation as little information exists on the excited states of $CaBH_4$. Ortiz[33] has calculated vibrational frequencies for the ground electronic state of $CaBH_4$. In this work, the frequency of the lateral motion of the borohydride ligand relative to the symmetry axis is predicted to be $528\ \text{cm}^{-1}$. This is within 20% of the $\tilde{A}\,^2A_1$-$\tilde{B}\,^2E_{1/2}$ separation ($\sim 638\ \text{cm}^{-1}$), making the first level of this vibration a possible candidate to be the perturbing state.

VI. CONCLUSION

A rotational analysis of the $\tilde{B}\,^2E$-$\tilde{X}\,^2A_1$ transitions of $CaBH_4$ and $SrBH_4$ has been completed. This analysis has yielded rotational and fine structure parameters for each observed state for the first time. No evidence for fluxional behavior due to the internal rotation of the BH_4^- ligand was found for either molecule. The rotational constants agree well with those calculated for a tridentate structure. A comparison of the molecular parameters of $CaBH_4$ and $SrBH_4$ with those of their monomethyl counterparts shows a large reduction in the spin-orbit separation and the metal-ligand separation upon electronic excitation. These suggest an increased amount of d-orbital character in the first excited ^2E state of the monoborohydrides as compared to the monomethyls of strontium and calcium, which is consistent with theoretical calculations. A reordering of the first excited ^2E and $^2A_1$ states has also been confirmed for $CaBH_4$ and $SrBH_4$ as compared to $CaCH_3$ and $SrCH_3$. Finally, the ambiguous J assignments of the rotational lines of the $^pP_{11}$ branch in the $\tilde{B}\,^2E_{1/2}$ spin-orbit component of $CaBH_4$ and the negative value of ε_{aa} suggest that this spin-orbit component is perturbed, most likely by a vibrational level of the $\tilde{A}\,^2A_1$ state.

ACKNOWLEDGMENT

Financial support for this work was provided by the Natural Sciences and Engineering Research Council (NSERC) of Canada.

[1] P. F. Bernath, *Advances in Photochemistry* (Wiley, New York, 1997), Vol. 23, p. 1.
[2] A. M. Ellis, Int. Rev. Phys. Chem. **20**, 551 (2001).
[3] C. M. Gittins, N. A. Harris, R. W. Field, J. Vergès, C. Effantin, A. Bernard, J. D'Incan, W. E. Ernst, P. Bündgen, and B. Engels, J. Mol. Spectrosc. **161**, 303 (1993).

[4] P. M. Sheridan, M. J. Dick, J.-G. Wang, and P. F. Bernath, J. Mol. Spectrosc. **233**, 269 (2005).
[5] M. J. Dick, P. M. Sheridan, J.-G. Wang, and P. F. Bernath, J. Chem. Phys. **124**, 174309 (2006).
[6] P. M. Sheridan, M. J. Dick, J.-G. Wang, and P. F. Bernath, J. Phys. Chem. A **109**, 10547 (2005).
[7] B. D. James and M. G. H. Wallbridge, Prog. Inorg. Chem. **11**, 99 (1970).
[8] T. J. Marks and J. R. Kolb, Chem. Rev. (Washington, D.C.) **77**, 263 (1977).
[9] Y. Kawashima, C. Yamada, and E. Hirota, J. Chem. Phys. **94**, 7707 (1991).
[10] Y. Kawashima and E. Hirota, J. Mol. Spectrosc. **153**, 466 (1992).
[11] Y. Kawashima, Y. Ohshima, Y. Endo, and E. Hirota, J. Mol. Spectrosc. **174**, 279 (1995).
[12] Y. Kawashima, O. N. Ulenikov, and E. Hirota, Mol. Phys. **101**, 623 (2003).
[13] Y. Kawashima and E. Hirota, J. Chem. Phys. **102**, 6961 (1995).
[14] Y. Kawashima and E. Hirota, J. Chem. Phys. **96**, 2460 (1992).
[15] E. Hirota and Y. Kawashima, J. Mol. Spectrosc. **181**, 352 (1997).
[16] W. C. Price, H. C. Longuet-Higgins, B. Rice, and T. F. Young, J. Chem. Phys. **17**, 217 (1949).
[17] W. C. Price, J. Chem. Phys. **17**, 1044 (1949).
[18] E. H. Coker and D. E. Hofer, J. Chem. Phys. **48**, 2713 (1968).
[19] A. I. Boldyrev, O. P. Charkin, N. G. Rambidi, and V. I. Avdeev, Chem. Phys. Lett. **44**, 20 (1976).
[20] J. D. Dill, P. v. R. Schleyer, J. S. Binkley, and J. A. Pople, J. Am. Chem. Soc. **99**, 6159 (1977).
[21] R. Bonaccorsi, E. Scrocco, and J. Tomasi, Theor. Chim. Acta **52**, 113 (1979).
[22] V. Barone, G. Dolcetti, F. Lelj, and N. Russo, Inorg. Chem. **20**, 1687 (1981).
[23] L. Y. Baranov and A. I. Boldyrev, Chem. Phys. Lett. **96**, 218 (1983).
[24] V. Kellö, M. Urban, and A. I. Boldyrev, Chem. Phys. Lett. **106**, 455 (1984).
[25] D. J. DeFrees, K. Raghavachari, H. B. Schlegel, J. A. Pople, and P. v. R. Schleyer, J. Phys. Chem. **91**, 1857 (1987).
[26] R. Bonaccorsi, O. P. Charkin, and J. Tomasi, Inorg. Chem. **30**, 2964 (1991).
[27] J. S. Francisco and I. H. Williams, J. Phys. Chem. **96**, 7567 (1992).
[28] V. V. Nefedova, A. I. Boldyrev, and J. Simons, J. Chem. Phys. **98**, 8801 (1993).
[29] E. Hirota, J. Mol. Spectrosc. **153**, 447 (1992).
[30] F. S. Pianalto, A. M. R. P. Bopegedera, W. T. M. L. Fernando, R. Hailey, L. C. O'Brien, C. R. Brazier, P. C. Keller, and P. F. Bernath, J. Am. Chem. Soc. **112**, 7900 (1990).
[31] C. R. Brazier and P. F. Bernath, J. Chem. Phys. **91**, 4548 (1989).
[32] A. J. Marr, F. Grieman, and T. C. Steimle, J. Chem. Phys. **105**, 3930 (1996).
[33] J. V. Ortiz, J. Am. Chem. Soc. **113**, 1102 (1991).
[34] W.-T. Chan and I. P. Hamilton, Chem. Phys. Lett. **316**, 171 (2000).
[35] C. Zhao, P. G. Hajigeorgiou, P. F. Bernath, and J. W. Hepburn, J. Mol. Spectrosc. **176**, 268 (1996).
[36] S. Gerstenkorn and P. Luc, *Atlas du Spectre d'Absorption de la Molécule d'Iode* (Laboratoire Aimé-Cotton, CNRS 91405 Orsay, France, 1978).
[37] A. M. R. P. Bopegedera, C. R. Brazier, and P. F. Bernath, J. Phys. Chem. **91**, 2779 (1987).
[38] A. M. R. P. Bopegedera, C. R. Brazier, and P. F. Bernath, J. Mol. Spectrosc. **129**, 268 (1988).
[39] M. Li and J. A. Coxon, J. Mol. Spectrosc. **176**, 206 (1996).
[40] M. J. Dick, P. M. Sheridan, J.-G. Wang, and P. F. Bernath, J. Mol. Spectrosc. **233**, 197 (2005).
[41] J. T. Hougen, J. Mol. Spectrosc. **81**, 73 (1980).
[42] J. M. Brown, Mol. Phys. **20**, 817 (1971).
[43] C. H. Townes and A. L. Schawlow, *Microwave Spectroscopy* (Dover, New York, 1975).
[44] M. A. Anderson, J. S. Robinson, and L. M. Ziurys, Chem. Phys. Lett. **257**, 471 (1996).
[45] M. A. Anderson and L. M. Ziurys, Astrophys. J. **460**, L77 (1996).
[46] Y. Endo, S. Saito, and E. Hirota, J. Chem. Phys. **81**, 122 (1984).
[47] See EPAPS Document No. E-JCPSA6-126-016716 for a complete list of the measured transition frequencies of the $\tilde{B}\,^2E$-$\tilde{X}\,^2A_1$ electronic transitions of $SrBH_4$ and $CaBH_4$. This document can be reached via a direct link in the online article's HTML reference section or via the EPAPS homepage (http://www.aip.org/pubservs/epaps.html).
[48] J.-G. Wang, P. M. Sheridan, M. J. Dick, and P. F. Bernath, J. Mol. Spectrosc. **236**, 21 (2006).
[49] G. Herzberg, *Electronic Spectra and Electronic Structure of Polyatomic Molecules*, Molecular Spectra and Molecular Structure Vol. III (Krieger, Malabar, 1991).
[50] T. M. Cerny, X. Q. Tan, J. M. Williamson, E. S. J. Robles, A. M. Ellis, and T. A. Miller, J. Chem. Phys. **99**, 9376 (1993).
[51] R. Rubino, J. M. Williamson, and T. A. Miller, J. Chem. Phys. **103**, 5964 (1995).
[52] H. Lefebvre-Brion and R. W. Field, *The Spectra and Dynamics of Diatomic Molecules* (Elsevier, Amsterdam, 2004).
[53] C. E. Moore, *Atomic Energy Levels*, Natl. Bur. Stand. Ref. Data Ser., Natl. Bur. Stand. (U.S.) Circ. No. 35 (U.S. GPO, Washington, D.C., 1971), p. 192 (strontium).
[54] C. E. Moore, *Atomic Energy Levels*, Natl. Bur. Stand. Ref. Data. Ser., Natl. Bur. Stand. (U.S.) Circ. No. 35, (U.S. GPO, Washington, DC, 1971), p. 246 (calcium).
[55] I. Kopp and J. T. Hougen, Can. J. Phys. **45**, 2581 (1967).
[56] R. N. Dixon, Mol. Phys. **10**, 1 (1965).